ADVANCED MATERIALS
www.advmat.de

Impact of Side-Chain Hydrophilicity on Packing, Swelling, and Ion Interactions in Oxy-Bithiophene Semiconductors

Nicholas Siemons, Drew Pearce, Camila Cendra, Hang Yu, Sachetan M. Tuladhar, Rawad K. Hallani, Rajendar Sheelamanthula, Garrett S. LeCroy, Lucas Siemons, Andrew J. P. White, Iain McCulloch, Alberto Salleo, Jarvist M. Frost, Alexander Giovannitti, and Jenny Nelson**

Exchanging hydrophobic alkyl-based side chains to hydrophilic glycol-based side chains is a widely adopted method for improving mixed-transport device performance, despite the impact on solid-state packing and polymer-electrolyte interactions being poorly understood. Presented here is a molecular dynamics (MD) force field for modeling alkoxylated and glycolated polythiophenes. The force field is validated against known packing motifs for their monomer crystals. MD simulations, coupled with X-ray diffraction (XRD), show that alkoxylated polythiophenes will pack with a "tilted stack" and straight interdigitating side chains, whilst their glycolated counterpart will pack with a "deflected stack" and an s-bend side-chain configuration. MD simulations reveal water penetration pathways into the alkoxylated and glycolated crystals—through the π-stack and through the lamellar stack respectively. Finally, the two distinct ways triethylene glycol polymers can bind to cations are revealed, showing the formation of a metastable single bound state, or an energetically deep double bound state, both with a strong side-chain length dependence. The minimum energy pathways for the formation of the chelates are identified, showing the physical process through which cations can bind to one or two side chains of a glycolated polythiophene, with consequences for ion transport in bithiophene semiconductors.

1. Introduction

Mixed ionic–electronic conducting conjugated polymers (organic mixed ionic–electronic conductors, OMIECs) underpin the operation of a range of bioelectronic devices,[1–3] such as organic electrochemical transistors (OECTs),[4–6] batteries,[7] and supercapacitors.[6] They have inherent advantages over traditional organic semiconductors for these electrochemical applications,[4,8–10] in particular their ability to operate with an aqueous electrolyte.[11,12] Exchanging a traditional alkyl-based side chain for a glycol-based hydrophilic side chain has been widely adopted as a strategy for increasing uptake of water and ions in OMIECs, and subsequently increasing their capacitance.[5,7,13–15] Whilst polythiophenes bearing long alkyl side chains are often reported to pack with interdigitating side chains[16–22] and π-stacks that are either straight or lightly tilted[17,20,22–24] (see Figure S1, Supporting Information for backbone packing motifs referred to in this study), little is known about glycolated OMIEC packing, despite the chain packing being critical to both electronic and ionic transport.[21,25–28]

Experimental studies have suggested that glycolated OMIECs adopt smaller π-stack distances than their alkylated counterparts.[5,29] As well as solid-state packing, structural characterization of OMIECs should account for their swelling behavior,

N. Siemons, D. Pearce, H. Yu, S. M. Tuladhar, J. M. Frost, J. Nelson
Department of Physics
Imperial College
London, Exhibition Rd, South Kensington, London SW7 2AZ, UK
E-mail: n.siemons18@imperial.ac.uk; jenny.nelson@imperial.ac.uk

C. Cendra, G. S. LeCroy, A. Salleo, A. Giovannitti
Department of Materials Science and Engineering
Stanford University
450 Serra Mall, Stanford, CA 94305, USA

The ORCID identification number(s) for the author(s) of this article can be found under https://doi.org/10.1002/adma.202204258.

DOI: 10.1002/adma.202204258

R. K. Hallani, R. Sheelamanthula
Physical Sciences and Engineering Division, KAUST Solar Center
King Abdullah University of Science and Technology (KAUST)
Thuwal 23955, Saudi Arabia

L. Siemons
Structural biology of cells and viruses laboratory
The Francis Crick Institute
1 Midland Road, London NW1 1AT, UK

A. J. P. White
Chemical Crystallography Laboratory
Department of Chemistry
Imperial College London White City Campus
82 Wood Lane, London W12 0BZ, UK

I. McCulloch
Department of Chemistry
University of Oxford
Oxford OX1 2JD, UK

since electrochemical doping is known to cause volumetric swelling in these systems.[27,30] XRD studies have thus correlated doping with an increase in lamellar stack spacing for both alkylated and glycolated polymers,[31–37] implying electrolyte entry into the lamellar stack. However, as the majority of the polymer is noncrystalline, X-ray diffraction (XRD) alone is unable to characterize many features critical to charge transport.[38–42] Furthermore, it is unable to determine the position of water and ions in the lattice beyond inferring it from the polymer structure. To obtain this level of detail it is necessary to use experimental methods such as solid-state nuclear magnetic resonance (ssNMR) crystallography,[43–45] or computational methods such as molecular dynamics (MD).

MD offers the means to simulate atomistic structure and dynamics for both ordered and amorphous polymers, as well as for liquids, but relies on careful force-field validation,[46–48] especially for π-conjugated systems.[49,50] Even with a validated force field, finding stable polymer crystal motifs with MD is challenging due to its limited sampling of the morphological phase space.[51–55] Therefore MD studies on the ordered phase of OMIECs have not attempted to identify packing structures but have ensured long-range order through use restraining potentials and small simulation cells,[56] or constraining systems to two dimensions.[57] Some studies[57–59] have taken advantage of MD's ability to probe amorphous polymer phases to uncover phase transitions during doping, however, they use the General AMBER Force Field[47] that has not been validated for the systems under study and is primarily designed for modeling of non-conjugated systems.[60] Other studies use the same force field,[61,62] but reparameterize backbone dihedrals to accurately capture backbone torsional behavior, a necessary step to accurately model the behavior of conjugated polymers.[60,63–65] Some of the latter work,[62] as well as studies in closely related fields using more advanced validated force fields,[66,67] have made progress on understanding electrolyte structure in polymer films, showing that hydrophilic side chains will coordinate with cations, with implications for the operation of both hole- and electron-transporting OMIECs.[68–72] MD studies to date however have not been used to calculate water placement in an ordered polymer lattice. Whilst MD studies have clearly shown the ability of cations to coordinate with glycol side chains, free-energetic quantities cannot safely be inferred from populations obtained from a limited sample of the morphology. For MD studies of binding events in biological systems,[73–79] it is generally accepted that enhanced sampling methods such as metadynamics[80–83] must be used to sufficiently sample the morphological phase space, and we propose the same is true in polymer systems.

To understand the packing behaviors of glycolated OMIECs, we have taken the archetypal glycolated polythiophene, poly(3,3'-dialkoxy(triethyleneglycol)-bithiophene) (p(gT2)),[7] and synthesized an alkylated analogue for comparison, poly(3,3'-dialkoxy(tetradecyl)-bithiophene) (p(aT2)). The oxygen atom at the side-chain attachment point is kept in the latter polymer, as it is known to strongly influence the backbone morphology and redox properties.[84] As a result, p(aT2) will be referred to as having "alkoxy" side chains.

To provide a means to validate a force field that can characterize the packing of p(aT2) and p(gT2) (see Section S2, Supporting Information for details on the force field), and to provide a starting point with which to find viable packing motifs for the polymers, monomer crystals of Sn-gT2 and Br-aT2 are synthesized, and their packing atomistically characterized with single crystal XRD.[85,86] We then proceed to investigate how the interaction with water, as well as water placement in the polymer lattice, depend on the chemistry of the side chain. Finally we observe and quantitatively characterize the ion–side-chain interactions that are unique to glycol side chains that have been intuitively known and only qualitatively studied thus far.

2. Results

Force-field validation is achieved through good agreement between simulated XRD powder patterns and experimental single-crystal XRD patterns for the monomer crystals, shown in **Figure 1**. The simulated supercells contain between 250 and 300 monomers and are stable throughout the MD simulation. They further show stability when annealed at 350 K, with the Br-aT2 crystal also stable after annealing at 400 K (Figure S9, Supporting Information), corroborating the experimental observation that Br-aT2 crystals are easier to grow than Sn-gT2 crystals. We see close agreement between experimental and simulated patterns, with almost all the peaks present in experiment being present in our simulated pattern. Additionally, relative peak intensities and widths are well reproduced, showing not only is the structure maintained, but also the relative levels of disorder between the crystallographic planes are reproduced.

Utilizing packing behaviors observed in the monomer crystals, we are able to hypothesize and test, in terms of stability, candidate crystal motifs for p(aT2) and p(gT2). For each candidate structure, a supercell of around 60 oligomers, each of 20 repeat units, is simulated for 50 ns using our validated force field. For the structures that maintained their long-range order, simulated XRD powder patterns are calculated and compared with experiment. After testing a variety of potential structures for both alkoxylated and glycolated crystals, those shown in **Figure 2** both show stability in our simulations, and closely reproduce the experimentally measured XRD patterns. In the case of p(aT2), an unusually large lamellar stack of 24.6 Å is observed experimentally, incongruent with an ordered dry polymer crystal with a maximum side chain of length 18 Å. We therefore suggest that there is residual solvent in the p(aT2) crystal phase such as that seen for the alkylated conjugated polymer PFO,[87,88] or thermal disorder leading to the expansion of the lamellar stack, such as that observed in polythiophenes with aliphatic side chains.[89]

The polymer XRD patterns derived from the MD simulations show peaks not seen in experiment that are associated with side-chain order (thin lines in Figure 2). Due to the close agreement between experimentally derived and simulated patterns where side-chain contributions are omitted (full red and orange lines in Figure 2), and the close match between simulated and experimental 2D GIWAXS patterns when side chains are excluded (Figures S13 and S14, Supporting Information), we conclude that the crystalline polymer phase shows some level of disorder amongst the side chains. Nevertheless, fitting the experimental peak widths to the peak order in the lamellar direction (Figures S15, Supporting Information) shows coherence over 4 and 8 lamellar

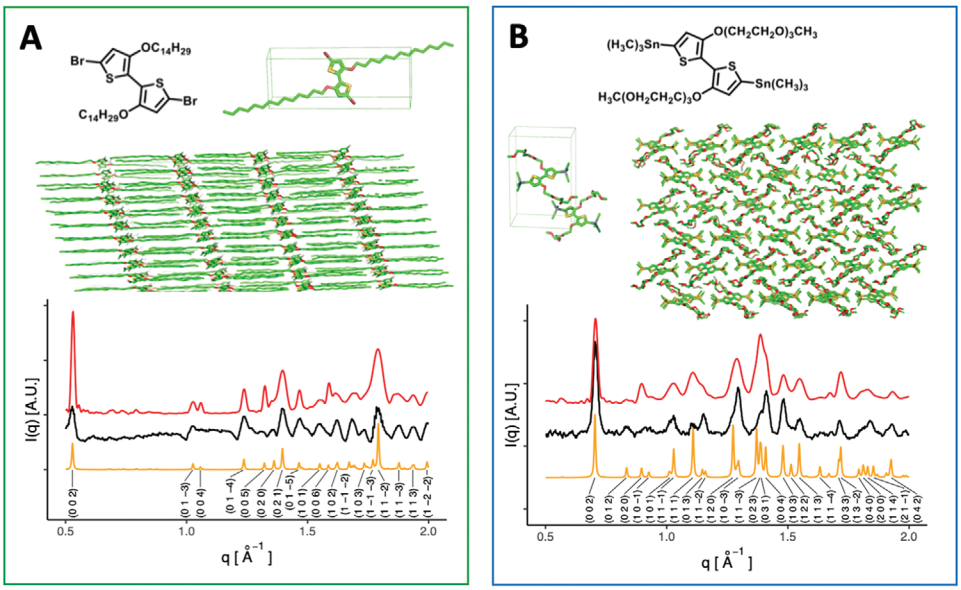

Figure 1. A,B) Monomer crystal determination through experimentation, and MD force-field validation with Br-aT2 (A) and Sn-gT2 (B). Each panel contains the chemical display formula of the molecule, an illustration of the unit cell and supercell, and the experimentally determined X-ray diffraction pattern (black line), as well as the simulated X-ray pattern from MD (red line) and the simulated pattern generated from the experimentally determined packing motif (orange line), calculated using the Bragg equation and allowing for peak index allocation. Unit cell parameters are $a = 4.17$ Å, $b = 9.30$ Å, $c = 23.80$ Å, $\alpha = 91.8°$, $\beta = 91.5°$, $\gamma = 96.5°$, P-1 symmetry for Br-aT2 and $a = 7.00$ Å, $b = 14.02$ Å, $c = 18.01$ Å, $\alpha = 90.00°$, $\beta = 97.71°$, $\gamma = 90.00°$, P21/n symmetry for Sn-gT2.

planes for p(aT2) and p(gT2) respectively, indicating sufficient side-chain ordering to maintain registration over multiple lamellae. Therefore peaks in experimental patterns, particularly at high $\vec{q}$ values, may still arise from side chains, or have additional intensity due to side-chain scattering.

The alkoxylated monomer and polymer crystals share similarities, showing the same symmetry elements and side-chain structure. The π-stacking structure is similar, with both crystals adopting a "tilted stack," and both crystals having straight interdigitating side chains. Stronger differences are observed

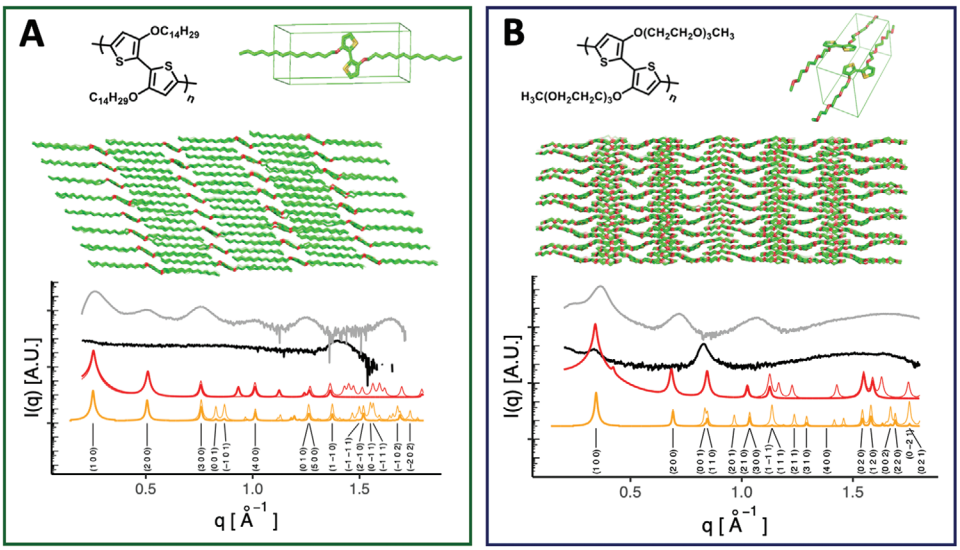

Figure 2. Polymer crystal determination for A) p(aT2) and B) p(gT2). Each panel contains the chemical display formula, an illustration of the unit cell and supercell, XRD patterns obtained from MD (red),[90,91] and the simulated pattern generated from the proposed packing motif (orange line), calculated using the Bragg equation and allowing for peak index allocation (see Section 4.2.2 for XRD pattern simulation details), experimental in-plane pattern (black) and experimental out-of-plane pattern (gray). See Figure S13, Supporting Information for 2D experimental spectra. The thin red and orange lines indicate peaks associated with the side chains, whilst the thick lines indicate those associated with the backbones. Unit cell parameters are $a = 22.4$ Å, $b = 5.3$ Å, $c = 7.6$ Å, $\alpha = 69°$, $\beta = 88°$, $\gamma = 86°$, P1 symmetry for p(aT2) and $a = 18.6$ Å, $b = 8.2$ Å, $c = 7.7$ Å, $\alpha = 90°$, $\beta = 70°$, $\gamma = 90°$, Pc symmetry for p(gT2).

between the glycolated monomer and polymer crystals. In the monomer, the side chains adopt a curled structure and no π-stacking is observed. For p(gT2), the side chains adopt a gentle s-bend configuration, and the backbones adopt a "deflected stack." In both cases however, the side chains arrange themselves so that oxygen atoms are neighbored by hydrogen atoms on other side chains.

When comparing the alkoxylated with the glycolated crystals, we see many differences in packing behavior. First, changing the side chain changes all parameters of the unit cell for both the monomer and polymer crystals. Second, the π-stacking characteristics are markedly different. In the case of p(aT2) the backbones adopt the "tilted stack" while p(gT2) adopts a "deflected stack." The (0 1 0) planes would indicate π-stacking separations of 5.2 and 4.0 Å for p(aT2) and p(gT2) respectively. Due to thermal disorder and crystal features such as a relatively acute α angle in the p(aT2) crystal, or the non-cofaciality of neighboring backbones in the p(gT2) crystal, the minimum distance between neighboring backbones can be as low as 3.4 and 3.3 Å respectively. In biological systems, this has been shown to be an important variable in modeling charge transfer rates.[41,42] Using this measure, as with the π-stacking distances, p(gT2) backbones are shown to pack more closely together.

Interesting features are found in the experimental XRD patterns which can be interpreted with knowledge of the packing motifs. In the case of p(gT2), the strong in-plane peak at $\vec{q} = 0.85$ Å^{-1} can be seen to arise from the (0 0 1) plane in the backbone direction, however due to the polymer film showing a level of mixed crystallite orientation (evident by some (1 0 0) scattering in the in-plane direction), it is possible that this peak has added intensity from the (1 1 0) peak. At q-values beyond $\vec{q} = 1.2$ Å^{-1}, peak allocation becomes difficult due to the high number of peaks in the structure factors and the possibility that side chains have sufficient order to scatter in this region, as discussed previously. However, a mixed-index peak is seen in p(gT2) at $\vec{q} = 1.12$Å^{-1} (arising from the (1 1 1) plane), which is strongly associated with the side chains. The absence of this peak in the experimental patterns, as well as simulation when side chains are omitted, again suggests disorder amongst the side chains of p(gT2). Furthermore, both simulated scattering intensities show that side chain ordering will have a significant effect on the intensity of the (0 0 1) family of planes, which are often strongly associated with the polymer backbones.

The polymer geometries provide a means to estimate the strength of electronic coupling between the conjugated backbones, which will strongly influence the rate of charge transport within crystalline regions of polymer films. Since both crystal structures have at least C2 symmetry, π-stack transfer integrals can be approximated via the energy-splitting-in-dimer method.[25,92] The p(aT2) transfer integrals are found to be 0.011 eV, and 0.059 eV for HOMO–HOMO and LUMO–LUMO couplings respectively when calculated for a pair of dimers using B3LYP functional and 6-311(g,p) basis set. For p(gT2), the HOMO–HOMO and LUMO–LUMO coupling transfer integrals are found to be 0.058 and 0.141 eV respectively.

To elucidate the effect of water exposure on the crystal structure, we immerse both alkoxylated and glycolated crystallites in water, the results of which are seen in **Figure 3**. In the case of the glycolated oligomers, water disrupts the crystalline packing, and in the case of Sn-gT2, the crystallite has begun to dissolve by the end of the simulation. For p(gT2), exposure to water causes the side chains to become less ordered, and their end

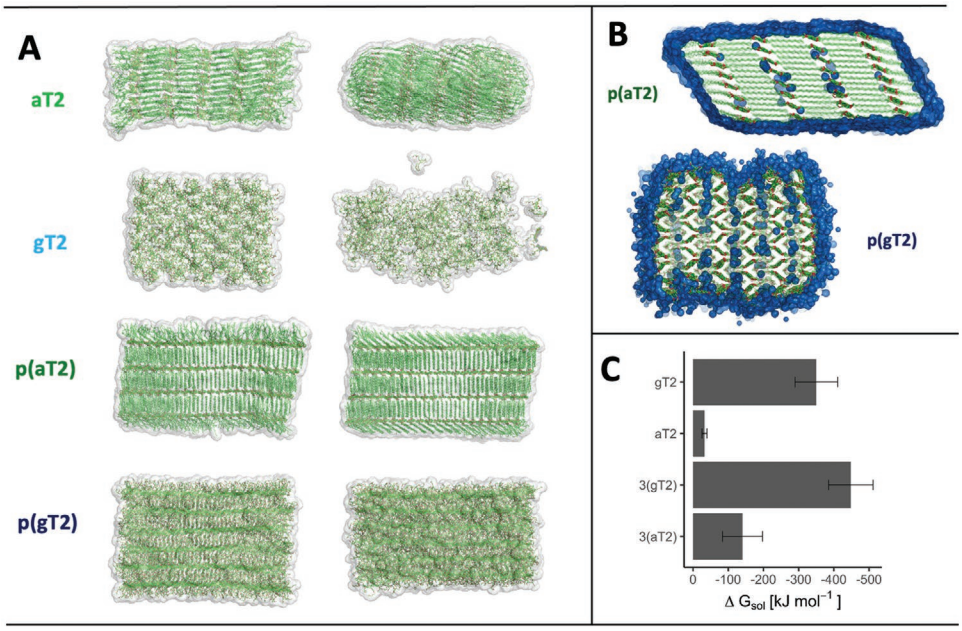

Figure 3. Structural response of crystallites upon exposure to water. A) Illustrations of the crystallites as viewed on the x–y plane after initial equilibration in MD (left column) and after 50 ns of simulation time (right column). The transparent surface indicates the solvent accessible surface areas of the crystallites. B) Cross-sections through the polymer crystallites, showing where and how the water enters, indicated by the blue surface. Side chains made partially transparent for clarity. C) Free energy of solvation of alkoxylated and glycolated oligomers presented in this study, calculated using MD (see Section S4.2.3, Supporting Information).

to end lengths shorten and generally adopt a curled structure, causing a reduction in the lamellar stack spacing. Alongside this, upon wetting of p(gT2), the "deflected stack" becomes more deflected, but overall the π-stack maintains structural order with a larger π-stack spacing of 6.0 nm (see Figure S17, Supporting Information). For Br-aT2 we see the monomers on the edge of the crystallite rearrange themselves so as to form a capsule, and reduce the area of the energetically unfavorable Br-aT2–water interface. In the center of the capsule the monomers are still arranged in a crystalline fashion, maintaining their side-chain interdigitation. In the case of p(aT2), the crystallite is undisturbed after wetting, with order being maintained in both the side chain and in the π-stack, and structural rearrangements of side chains only occurring on the surface of the crystallite. The relative effect of water on the crystals is quantitatively understood from the solvation free energies (Figure 3C), where hydrophilic species typically have three times or more the solvation free energy of their hydrophobic counterparts.

Water is seen to penetrate into both polymer crystallites, with about four times more water entering the glycolated crystallite in the 50 ns simulation, as seen in Figure 3B. In the case of p(gT2) the water enters the lamellar stack, residing amongst the hydrophilic side chains. Upon inspection it is seen that the water molecules typically sit with their hydrogens coordinating with glycol oxygen atoms, indicating hydrogen bonding occurring in the lamellar stack. Similar behavior has been observed for poly(ethylene oxide) solutions[93] and in biological environments.[94–96] For p(aT2), the water resides close to the backbone, furthest from the hydrophobic side chains. Simulations of bulk wet crystals (see Figure S18, Supporting Information) corroborate this observation, showing water droplet formation around the backbone for p(aT2), with each droplet containing around 30 water molecules. These simulations also show that water in crystalline p(gT2) is able to diffuse four times more quickly than in crystalline p(aT2), and both these diffusion rates are two orders of magnitude smaller than the self-diffusion of water.[97]

It has been observed experimentally that upon charging of a hole-transporting OMIEC, mass uptake is preceded by mass expulsion, implying the presence of cations in the bulk before doping.[69,70] Therefore the impact of ions on the structure of hole-transporting conjugated polymers should be understood. In order to test the ability of our simulations to correctly reproduce polymer–ion interactions, we first attempted to model the complexes formed between sodium or potassium cations and crown-ether bearing bithiophenes, for which solved crystal structures had previously been obtained. We used this as a test of our force field to correctly model cation chelation in similar materials (Figure S10, Supporting Information).[98] In all cases, our simulations are able to reproduce the experimentally determined crystal structures. We therefore proceeded to simulate p(aT2) and p(gT2) crystallites immersed in aqueous 0.2 M NaCl. The simulations suggest that cations, in the presence of glycol side chains, are becoming localized in space for periods of time, leading to small areas of high cation density (**Figure 4**A). On

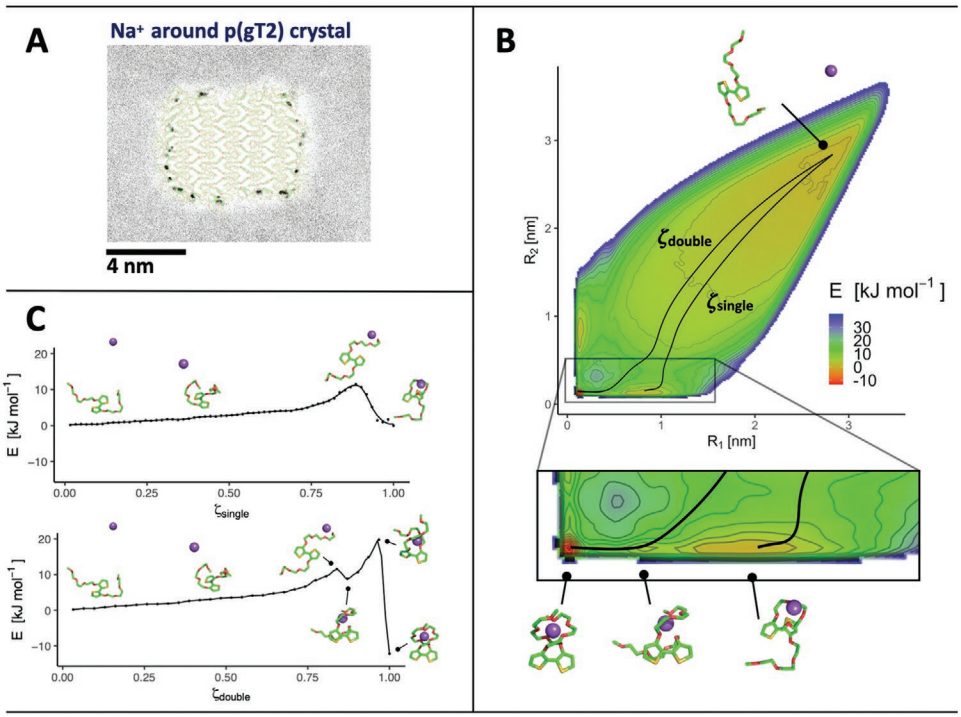

Figure 4. A) Density plots over the 50 ns production run of Na ions in the p(gT2) crystallite simulation, with the polymer crystallite shown in the center of the box. Darker areas indicate higher cation density. B) The free energy surface of the cation as a function of its distance from a glycol side chain on one side of the polymer (R_1), and its distance to a side chain on the other side of the polymer (R_2), with the solvated state shown. The black lines show the minimum energy pathways from the solvated state to the single bound state (ζ_{single}) and double bound state (ζ_{double}). The inset shows an area of the FES containing the single bound state, double bound state, and a locally stable transition state. C) The free-energy profiles for the transition from the solvated state to the single and double bound states along their optimal path, with illustrations of the bound and transition state configurations.

inspection we see that this is due to cation–side-chain chelation, such as those found for the crown-ether bithiophenes.[98] No such trapping effect is seen for anions, or for cations with the p(aT2) crystal.

To deepen our understanding of how cations could insert themselves into a crystalline lattice, we quantitatively study cation-glycol chelation using Metadynamics,[99–101] as shown in Figure 4B. A free energy surface (FES) is calculated as a function of the distance of the ion from a side chain on each thiophene unit (R_1 and R_2) within the bithiophene repeat unit (see Section S4.2.7, Supporting Information for more details on Metadynamics simulations). In the free energy landscape four notable states are identified. The first being the solvated state at high R_1 and R_2. Two shallow local minima are observed at $R_1 = 0.1$ nm or $R_2 = 0.1$ nm, corresponding to single bound metastable states to a single side chain with binding energy of -0.01 ± 0.07 kJ mol^{-1}. Finally a stable state is seen at $R_1 = 0.1$nm and $R_2 = 0.1$nm, corresponding to the ion being double bound to both side chains with energy of -13.3 ± 0.2 kJ mol^{-1}.

Shown in Figure 4C are minimum energy transition pathways from the solvated state to the bound states along reaction coordinates ζ_{single} and ζ_{double}. We see that for the formation of the double bound state, a larger energy barrier must be overcome compared to the single bound state (18.5 ± 0.4 kJ mol^{-1} compared to 11.5 ± 0.4 kJ mol^{-1}), which can be attributed to the requirement for the backbone to twist and the entropic penalty associated with fitting a second side chain around an ion. We also simulated the interactions between glycol side chains and the anion, and no notable states were seen (Figure S25, Supporting Information). Finally, a strong dependence of binding energy is seen with side-chain length (Figure S19, Supporting Information), in particular between triethylene and tetraethylene glycol whereby the single bound state goes from metastable to stable, and the double bound state goes from stable to unstable.

3. Discussion

Whilst simulations do not show ions entering the crystallites on the sub 100 ns time scale, metadynamics suggests potential ionic structure and dynamics. In the case of polythiophenes with tail-to-tail side-chain attachment, like those studied here, the double bound state requires the twisting of the backbone. This makes them unlikely to form in the crystalline phase due to the stabilizing π–π interactions and steric factors making the backbone twist energy barrier prohibitively large. As the single bound states are only metastable and have an energy barrier within the range of thermal energies, ion–glycol chelations would represent no significant ion transport trap in the crystalline phase for triethylene glycol. However, in the case of tetraethylene glycol, the single bound state is much deeper (see Figure S19, Supporting Information), and so cation trapping in the crystalline phase of tetraethylene glycol polymers is possible. Whilst we would expect both anions and cations to be in the polymer bulk after water exposure, cations would experience trapping, the strength of which would depend on the side-chain length as demonstrated here.

Comparison of the structural response of Sn-gT2 and p(gT2) upon wetting has revealed the importance of the π–π interactions in stabilizing the crystal structure of hydrophilic OMIECs. Whilst the driving forces for formation of the p(gT2) crystallite are both π–π interactions and electrostatics, for Sn-gT2 it is only the latter due to the absence of π-stacking. The dipole interactions are rapidly screened when water is present, thus leading to the rapid dissolution of the Sn-gT2 crystallite, and likely also leading to molecular-weight dependence of stability of the structure in water. Once the water has entered the lamellar stack for p(gT2), it is surprising that the backbones retain their long range order, whilst the side chains adopt a relatively amorphous structure with the intercalated water. Such structure could be described as a crystalline gel, where the crystalline backbones form the interconnecting element, and side chains and water form the gel phase.[102] The move to an amorphous morphology of the side chains causes a reduction in the lamellar stack, and an increase in the π-stack distance. For the hydrophobic crystallite we see some diffusion of water into the crystal. This is possibly enhanced by the use of alkoxy side chains rather than alkyl. Furthermore, if the water enters the p(aT2) crystallite along the backbone, we might expect water entry to be suppressed if the crystallite is surrounded by amorphous bulk polymer, as these narrow channels would become fully or partially blocked.

Whilst in the solid state some hydrophobic conjugated polymers with short side chains have been shown to adopt lightly "tilted stacks",[103–106] the majority of polythiophenes have been shown to adopt "straight stacks".[23,24,43,107–109] It is interesting therefore, that the exchange from an alkyl to an alkoxy side chain induces a significant tilt in the π-stack. This is possibly due to the electrostatic repulsion of the oxygen atoms in the alkoxy side chain, as well as the increased rotational freedom around the base of the side chain associated with exchanging CH_2 groups for oxygen.[29] Transitioning to a glycol side chain causes the backbones to adopt a "deflected stack". We note that the glycol crystal more closely resembles an ionic lattice, such that negatively charged atoms are placed in the lamellar stack opposite positively charged ones. The added strain applied to the system to satisfy this requirement is likely influencing the resulting backbone stacking motif. Whilst in the monomer crystal the hydrophilic side chains adopt a curled structure, in the polymer they adopt a gentle s-bend configuration. We expect the monomer end caps to play a role in determining the overall monomer packing behaviors, for example the bulky $Sn(Me)_3$ end caps lower the effective side-chain attachment density of the monomers and over-all hydrophilicity of the medium. However, the choice of monomer end-cap should not affect the packing of the polymer. These factors may lead to observed differences in side-chain conformation between Sn-gT2 monomer and p(gT2) polymer.

The change in backbone packing when exchanging alkoxy for glycol side chains leads to a higher inter-backbone electronic transfer integral. Given that charge transport is likely dominated by intermolecular charge transfer,[110] we would propose that, if the impact of side-chain type on electrostatic interactions can be neglected, a perfect dry glycolated crystal is better suited to electronic charge transport than an alkoxylated one. However, our simulations do not sample the crystalline imperfections shown by the broad peaks in the XRD pattern, nor the presence of any residual solvents that may be leading to an enlarged lamellar stack. Both of these are likely to influence electronic charge transport in these systems.

Glycol side chains have been used extensively to improve OMIEC device performance, despite issues remaining around device stabilities during electrochemical cycling. Already design strategies have been proposed to negate these side effects, and usually revolve around altering side-chain lengths,[61,111] attachment positions,[112] or combining hydrophobic and hydrophilic moieties.[5,56] [113,114] In all these cases the amorphous phase, as well as the crystalline phase, is likely to be important in maintaining structural integrity of films. Our force field opens up the opportunity to atomistically characterize structural packing and probe the short range order and interactions in the amorphous phase when these chemical designs are applied.

4. Conclusion

We have atomistically characterized the polymer packing of archetypal alkoxy and glycolated polythiophene polymers. We uncovered the changes in packing behaviors to accommodate the side chains of different chemistries, in particular the adoption of either a "straight stack," "tilted stack," or a more densely packed "deflected stack" depending on the oxygen content of the side chains. These behaviors indicate the glycolated polymers pack more effectively for optimizing charge transport in the solid state. We have subsequently observed the response of the polymer to water exposure, as well as the placement of water in the polymer lattices—around the backbone for alkoxy systems, and in the lamellar stack for glycol systems. We have shown the important effects of π–π interactions in stabilizing the polymer lattice, demonstrating that enhancing the π-stacking in systems is critical to ensuring their stability in aqueous environments, with implications for optimizing polymer molecular weights. Finally, metadynamics has revealed that triethylene glycol side chains are the optimum length for ensuring no cation trapping in the crystalline phase of OMIECs, whilst tetraethylene glycol is more suited to applications where cation trapping is desirable. Studies on these materials using atomistic and quantitative molecular simulations coupled with experimental characterization, as followed here, is valuable for guiding future polymer OMIEC design.

Supporting Information

Supporting Information is available from the Wiley Online Library or from the author.

Acknowledgements

J.N., N.S., D.P., and A.G. acknowledge funding from the European Research Council (ERC) under the European Union's Horizon 2020 research and innovation program (grant agreement no. 742708, project CAPaCITy). H.Y. acknowledges support of the Chinese Scholarship Council through a Ph.D. studentship. S.M.T. acknowledges support from the UK Engineering and Physical Sciences Research Council via the Global Challenges Research Fund through the "SUNRISE" project. J.N. thanks the Royal Society for award of a Research Professorship. J.M.F. is supported by a Royal Society University Research Fellowship (URF-R1-191292). C.C. gratefully acknowledges financial support from the National Science Foundation DMR Award (no. 1808401). A.G. acknowledges funding from the TomKat Center for Sustainable Energy at Stanford University. G.L. acknowledges support from the National Science Foundation Graduate Research Fellowship Program under grant DGE-1656518. R.S. , R.K.H., and I.M. acknowledge financial support from KAUST, Office of Sponsored Research (OSR) awards no. OSR-2019-CRG8-4086 and OSR-2018-CRG7-3749. R.S. , R.K.H., and I.M. acknowledge funding from the European Union's Horizon 2020 research and innovation program under grant agreement no. 952911, project BOOSTER and grant agreement no. 862474, project RoLAFLEX, EPSRC Project EP/T026219/1 as well as EPSRC Project EP/T004908/1. All the authors would like to acknowledge Christopher Takacs at the SLAC National Accelerator Laboratory for useful discussions about polymer crystalline polymorphs and interpretation of experimental diffraction patterns.

Conflict of Interest

The authors declare no conflict of interest.

Data Availability Statement

The data that support the findings of this study are available from the corresponding author upon reasonable request.

Keywords

aqueous electrolytes, bioelectronics, conjugated polymers, mixed electronic/ionic conductors, molecular dynamics, organic mixed ionic–electronic conductors

Received: May 11, 2022
Revised: July 28, 2022
Published online: August 28, 2022

[1] J. Rivnay, S. Inal, A. Salleo, R. M. Owens, M. Berggren, G. G. Malliaras, *Nat. Rev. Mater.* **2018**, *3*, 17086.
[2] R. M. Owens, G. G. Malliaras, *MRS Bull.* **2010**, *35*, 449.
[3] M. Moser, J. F. Ponder Jr., A. Wadsworth, A. Giovannitti, I. McCulloch, *Adv. Funct. Mater.* **2019**, *29*, 1807033.
[4] L. R. Savagian, A. M. Österholm, J. F. Ponder Jr., K. J. Barth, J. Rivnay, J. R. Reynolds, *Adv. Mater.* **2018**, *30*, 1804647.
[5] A. Giovannitti, I. P. Maria, D. Hanifi, M. J. Donahue, D. Bryant, K. J. Barth, B. E. Makdah, A. Savva, D. Moia, M. Zetek, P. R. Barnes, O. G. Reid, S. Inal, G. Rumbles, G. G. Malliaras, J. Nelson, J. Rivnay, I. McCulloch, *Chem. Mater.* **2018**, *30*, 2945.
[6] A. Giovannitti, D. T. Sbircea, S. Inal, C. B. Nielsen, E. Bandiello, D. A. Hanifi, M. Sessolo, G. G. Malliaras, I. McCulloch, J. Rivnay, *Proc. Natl. Acad. Sci. USA* **2016**, *113*, 12017.
[7] D. Moia, A. Giovannitti, A. A. Szumska, I. P. Maria, E. Rezasoltani, M. Sachs, M. Schnurr, P. R. Barnes, I. McCulloch, J. Nelson, *Energy Environ. Sci.* **2019**, *12*, 1349.
[8] J. Rivnay, S. Inal, B. A. Collins, M. Sessolo, E. Stavrinidou, X. Strakosas, C. Tassone, D. M. Delongchamp, G. G. Malliaras, *Nat. Commun.* **2016**, *7*, 11287.
[9] C. B. Nielsen, A. Giovannitti, D. T. Sbircea, E. Bandiello, M. R. Niazi, D. A. Hanifi, M. Sessolo, A. Amassian, G. G. Malliaras, J. Rivnay, I. McCulloch, *J. Am. Chem. Soc.* **2016**, *138*, 10252.
[10] Y. Wang, E. Zeglio, H. Liao, J. Xu, F. Liu, Z. Li, I. P. Maria, D. Mawad, A. Herland, I. McCulloch, W. Yue, *Chem. Mater.* **2019**, *31*, 9797.
[11] A. M. Pappa, D. Ohayon, A. Giovannitti, I. P. Maria, A. Savva, I. Uguz, J. Rivnay, I. McCulloch, R. M. Owens, S. Inal, *Sci. Adv.* **2018**, *4*, eaat0911.

[12] D. Ohayon, G. Nikiforidis, A. Savva, A. Giugni, S. Wustoni, T. Palanisamy, X. Chen, I. P. Maria, E. Di Fabrizio, P. M. Costa, I. McCulloch, S. Inal, *Nat. Mater.* **2019**, *19*, 456.
[13] R. Kroon, D. Kiefer, D. Stegerer, L. Yu, M. Sommer, C. Müller, *Adv. Mater.* **2017**, *29*, 1700930.
[14] D. Kiefer, A. Giovannitti, H. Sun, T. Biskup, A. Hofmann, M. Koopmans, C. Cendra, S. Weber, L. J. Anton Koster, E. Olsson, J. Rivnay, S. Fabiano, I. McCulloch, C. Müller, *ACS Energy Letters* **2018**, *3*, 278.
[15] X. Chen, A. Marks, B. D. Paulsen, R. Wu, R. B. Rashid, H. Chen, M. Alsufyani, J. Rivnay, I. McCulloch, *Angew. Chem., Int. Ed.* **2021**, *60*, 9368.
[16] R. J. Kline, D. M. DeLongchamp, D. A. Fischer, E. K. Lin, L. J. Richter, M. L. Chabinyc, M. F. Toney, M. Heeney, I. McCulloch, *Macromolecules* **2007**, *40*, 7960.
[17] T. Prosa, M. Winokur, R. McCullough, *Macromolecules* **1996**, *29*, 3654.
[18] P. Keg, A. Lohani, D. Fichou, Y. M. Lam, Y. Wu, B. S. Ong, S. G. Mhaisalkar, *Macromol. Rapid Commun.* **2008**, *29*, 1197.
[19] J. Mei, Z. Bao, *Chem. Mater.* **2014**, *26*, 604.
[20] D. M. DeLongchamp, R. J. Kline, E. K. Lin, D. A. Fischer, L. J. Richter, L. A. Lucas, M. Heeney, I. McCulloch, J. E. Northrup, *Adv. Mater.* **2007**, *19*, 833.
[21] I. McCulloch, M. Heeney, C. Bailey, K. Genevicius, I. MacDonald, M. Shkunov, D. Sparrowe, S. Tierney, R. Wagner, W. Zhang, M. L. Chabinyc, R. J. Kline, M. D. McGehee, M. F. Toney, *Nat. Mater.* **2006**, *5*, 328.
[22] M. L. Chabinyc, M. F. Toney, R. J. Kline, I. McCulloch, M. Heeney, *J. Am. Chem. Soc.* **2007**, *129*, 3226.
[23] K. Tashiro, M. Kobayashi, T. Kawai, K. Yoshino, *Polymer* **1997**, *38*, 2867.
[24] M. J. Winokur, P. Wamsley, J. Moulton, P. Smith, A. J. Heeger, *Macromolecules* **1991**, *24*, 3812.
[25] V. Coropceanu, J. Cornil, D. A. da Silva Filho, Y. Olivier, R. Silbey, J.-L. Brédas, *Chem. Rev.* **2007**, *107*, 926.
[26] H. R. Tseng, H. Phan, C. Luo, M. Wang, L. A. Perez, S. N. Patel, L. Ying, E. J. Kramer, T. Q. Nguyen, G. C. Bazan, A. J. Heeger, *Adv. Mater.* **2014**, *26*, 2993.
[27] L. Q. Flagg, C. G. Bischak, J. W. Onorato, R. B. Rashid, C. K. Luscombe, D. S. Ginger, *J. Am. Chem. Soc.* **2019**, *141*, 4345.
[28] S.-M. Kim, C.-H. Kim, Y. Kim, N. Kim, W.-J. Lee, E.-H. Lee, D. Kim, S. Park, K. Lee, J. Rivnay, M.-H. Yoon, *Nat. Commun.* **2018**, *9*, 3858.
[29] B. Meng, H. Song, X. Chen, Z. Xie, J. Liu, L. Wang, *Macromolecules* **2015**, *48*, 4357.
[30] A. Savva, R. Hallani, C. Cendra, J. Surgailis, T. C. Hidalgo, S. Wustoni, R. Sheelamanthula, X. Chen, M. Kirkus, A. Giovannitti, A. Salleo, I. McCulloch, S. Inal, *Adv. Funct. Mater.* **2020**, *30*, 1907657.
[31] T. Kawai, M. Nakazono, K. Yoshino, *J. Mater. Chem.* **1992**, *2*, 903.
[32] J. O. Guardado, A. Salleo, *Adv. Funct. Mater.* **2017**, *27*, 1701791.
[33] J. L. Thelen, S. L. Wu, A. E. Javier, V. Srinivasan, N. P. Balsara, S. N. Patel, *ACS Macro Lett.* **2015**, *4*, 1386.
[34] E. M. Thomas, M. A. Brady, H. Nakayama, B. C. Popere, R. A. Segalman, M. L. Chabinyc, *Adv. Funct. Mater.* **2018**, *28*, 1803687.
[35] A. Savva, C. Cendra, A. Giugni, B. Torre, J. Surgailis, D. Ohayon, A. Giovannitti, I. McCulloch, E. Di Fabrizio, A. Salleo, J. Rivnay, S. Inal, *Chem. Mater.* **2019**, *31*, 927.
[36] C. Cendra, A. Giovannitti, A. Savva, V. Venkatraman, I. McCulloch, A. Salleo, S. Inal, J. Rivnay, *Adv. Funct. Mater.* **2019**, *29*, 1807034.
[37] B. D. Paulsen, A. Giovannitti, R. Wu, J. Strzalka, Q. Zhang, J. Rivnay, C. J. Takacs, *Small* **2021**, *17*, 2103213.
[38] B. Baumeier, J. Kirkpatrick, D. Andrienko, *Phys. Chem. Chem. Phys.* **2010**, *12*, 11103.
[39] E. F. Valeev, V. Coropceanu, D. A. Da Silva Filho, S. Salman, J. L. Brédas, *J. Am. Chem. Soc.* **2006**, *128*, 9882.
[40] J. Nelson, J. J. Kwiatkowski, J. Kirkpatrick, J. M. Frost, *Acc. Chem. Res.* **2009**, *42*, 1768.
[41] J. R. Winkler, A. J. Di Bilio, N. A. Farrow, J. H. Richards, H. B. Gray, *Pure Appl. Chem.* **1999**, *71*, 1753.
[42] C. C. Page, C. C. Moser, X. Chen, P. L. Dutton, *Nature* **1999**, *402*, 47.
[43] D. Dudenko, A. Kiersnowski, J. Shu, W. Pisula, D. Sebastiani, H. W. Spiess, M. R. Hansen, *Angew. Chem.* **2012**, *124*, 11230.
[44] F. Taulelle, *Solid State Sci.* **2004**, *6*, 1053.
[45] R. K. Harris, R. E. Wasylishen, M. J. Duer, *NMR Crystallography*, Vol. *4*, Wiley, New York **2009**.
[46] W. L. Jorgensen, D. S. Maxwell, J. Tirado-Rives, *J. Am. Chem. Soc.* **1996**, *118*, 11225.
[47] J. Wang, R. M. Wolf, J. W. Caldwell, P. A. Kollman, D. A. Case, *J. Comput. Chem.* **2004**, *25*, 1157.
[48] A. J. Stone, *The Theory of Intermolecular Forces*, Clarendon, Oxford, UK **1996**.
[49] M. Moreno, M. Casalegno, G. Raos, S. V. Meille, R. Po, *J. Phys. Chem. B* **2010**, *114*, 1591.
[50] R. S. Bhatta, Y. Y. Yimer, D. S. Perry, M. Tsige, *J. Phys. Chem. B* **2013**, *117*, 10035.
[51] F. Giberti, M. Salvalaglio, M. Mazzotti, M. Parrinello, *Chem. Eng. Sci.* **2015**, *121*, 51.
[52] F. Giberti, M. Salvalaglio, M. Parrinello, *Int. Union Crystallogr. J.* **2015**, *2*, 256.
[53] C. Liu, J. G. Brandenburg, O. Valsson, K. Kremer, T. Bereau, *Soft Matter* **2020**, *16*, 9683.
[54] P. M. Piaggi, M. Parrinello, *Proc. Natl. Acad. Sci. USA* **2018**, *115*, 10251.
[55] T. Zykova-Timan, P. Raiteri, M. Parrinello, *J. Phys. Chem. B* **2008**, *112*, 13231.
[56] J. Liu, G. Ye, H. G. Potgieser, M. Koopmans, S. Sami, M. I. Nugraha, D. R. Villalva, H. Sun, J. Dong, X. Yang, X. Qiu, C. Yao, G. Portale, S. Fabiano, T. D. Anthopoulos, D. Baran, R. W. A. Havenith, R. C. Chiechi, L. J. Anton Koster, *Adv. Mater.* **2021**, *33*, 2006694.
[57] S. Ghosh, I. Zozoulenko, *ACS Appl. Electron. Mater.* **2020**, *2*, 4034.
[58] J. Gladisch, E. Stavrinidou, S. Ghosh, A. Giovannitti, M. Moser, I. Zozoulenko, I. McCulloch, M. Berggren, *Adv. Sci.* **2019**, *7*, 1901144.
[59] M. Moser, J. Gladisch, S. Ghosh, T. C. Hidalgo, J. F. PonderJr, R. Sheelamanthula, Q. Thiburce, N. Gasparini, A. Wadsworth, A. Salleo, S. Inal, M. Berggren, I. Zozoulenko, E. Stavrinidou, I. McCulloch, *Adv. Funct. Mater.* **2021**, *31*, 2100723.
[60] K. H. DuBay, M. L. Hall, T. F. Hughes, C. Wu, D. R. Reichman, R. A. Friesner, *J. Chem. Theory Comput.* **2012**, *8*, 4556.
[61] M. Moser, L. R. Savagian, A. Savva, M. Matta, J. F. Ponder Jr, T. C. Hidalgo, D. Ohayon, R. Hallani, M. Reisjalali, A. Troisi, A. Wadsworth, J. R. Reynolds, S. Inal, I. McCulloch, *Chem. Mater.* **2020**, *32*, 6618.
[62] M. Matta, R. Wu, B. D. Paulsen, A. J. Petty, R. Sheelamanthula, I. McCulloch, G. C. Schatz, J. Rivnay, *Chem. Mater.* **2020**, *32*, 7301.
[63] J. Wildman, P. Repiscak, M. J. Paterson, I. Galbraith, *J. Chem. Theory Comput.* **2016**, *12*, 3813.
[64] V. Sundaram, A. V. Lyulin, B. Baumeier, *J. Phys. Chem. B* **2020**, *124*, 11030.
[65] C. M. Wolf, L. Guio, S. Scheiwiller, V. Pakhnyuk, C. Luscombe, L. D. Pozzo, *ACS Polym. Au* **2021**, *1*, 134.
[66] B. M. Savoie, M. A. Webb, T. F. Miller, *J. Phys. Chem. Lett.* **2017**, *8*, 641.
[67] A. Khot, B. M. Savoie, *J. Polym. Sci.* **2021**, *60*, 610.
[68] S. Wang, F. Li, A. D. Easley, J. L. Lutkenhaus, *Nat. Mater.* **2019**, *18*, 69.
[69] L. Q. Flagg, C. G. Bischak, R. J. Quezada, J. W. Onorato, C. K. Luscombe, D. S. Ginger, *ACS Mater. Lett.* **2020**, *2*, 254.
[70] Q.-X. Zhou, C. J. Kolaskie, L. L. Miller, *J. Electroanal. Chem. Interfacial Electrochem.* **1987**, *223*, 283.
[71] F. Chao, J. Baudoin, M. Costa, P. Lang, in *Makromolekulare Chemie. Macromolecular Symposia*, Vol. *8*, Wiley, New York **1987**, pp. 173–194.
[72] B. D. Paulsen, K. Tybrandt, E. Stavrinidou, J. Rivnay, *Nat. Mater.* **2020**, *19*, 13.

[73] V. Limongelli, M. Bonomi, M. Parrinello, *Proc. Natl. Acad. Sci. USA* **2013**, *110*, 6358.
[74] F. Moraca, J. Amato, F. Ortuso, A. Artese, B. Pagano, E. Novellino, S. Alcaro, M. Parrinello, V. Limongelli, *Proc. Natl. Acad. Sci. USA* **2017**, *114*, E2136.
[75] L. Troussicot, F. Guillière, V. Limongelli, O. Walker, J.-M. Lancelin, *J. Am. Chem. Soc.* **2015**, *137*, 1273.
[76] A. Barducci, R. Chelli, P. Procacci, V. Schettino, F. L. Gervasio, M. Parrinello, *J. Am. Chem. Soc.* **2006**, *128*, 2705.
[77] D. Granata, C. Camilloni, M. Vendruscolo, A. Laio, *Proc. Natl. Acad. Sci. USA* **2013**, *110*, 6817.
[78] A. J. Clark, P. Tiwary, K. Borrelli, S. Feng, E. B. Miller, R. Abel, R. A. Friesner, B. J. Berne, *J. Chem. Theory Comput.* **2016**, *12*, 2990.
[79] N. Saleh, P. Ibrahim, G. Saladino, F. L. Gervasio, T. Clark, *J. Chem. Inf. Model.* **2017**, *57*, 1210.
[80] P. Tiwary, A. van de Walle, in *Multiscale Materials Modeling for Nanomechanics*, Springer, Cham, Switzerland **2016**, pp. 195–221.
[81] R. C. Bernardi, M. C. Melo, K. Schulten, *Biochim. Biophys. Acta* **2015**, *1850*, 872.
[82] E. Paquet, H. L. Viktor, *BioMed Res. Int.* **2015**, *2015*, 183918.
[83] R. Elber, *Curr. Opin. Struct. Biol.* **1996**, *6*, 232.
[84] K. J. Thorley, I. McCulloch, *J. Mater. Chem. C* **2018**, *6*, 12413.
[85] G. M. Sheldrick, *Acta Crystallogr. Sect. A: Found. Adv.* **2015**, *71*, 3.
[86] Bruker, A. X. S., SAINT Software Reference Manual, Madison, WI, USA **1998**, *5465*.
[87] A. Perevedentsev, P. N. Stavrinou, D. D. Bradley, P. Smith, *J. Polym. Sci., Part B: Polym. Phys.* **2015**, *53*, 1481.
[88] A. Perevedentsev, P. N. Stavrinou, P. Smith, D. D. Bradley, *J. Polym. Sci., Part B: Polym. Phys.* **2015**, *53*, 1492.
[89] J. Liu, G. Ye, H. G. O. Potgieser, M. Koopmans, S. Sami, M. I. Nugraha, D. R. Villalva, H. Sun, J. Dong, X. Yang, X. Qiu, C. Yao, G. Portale, S. Fabiano, T. D. Anthopoulos, D. Baran, R. W. A. Havenith, R. C. Chiechi, L. J. A. Koster, *Adv. Mater.* **2020**, *33*, 2006694.
[90] W. M., Debyer package (**2011**), https://debyer.readthedocs.io/en/latest/ (accessed: May 2021).
[91] B. Hess, C. Kutzner, D. Van Der Spoel, E. Lindahl, *J. Chem. Theory Comput.* **2008**, *4*, 435.
[92] T. Koopmans, *Physica* **1934**, *1*, 104.
[93] G. D. Smith, D. Bedrov, O. Borodin, *Phys. Rev. Lett.* **2000**, *85*, 5583.
[94] J. Brady, R. Schmidt, *J. Phys. Chem.* **1993**, *97*, 958.
[95] C. F. Lopez, S. O. Nielsen, M. L. Klein, P. B. Moore, *J. Phys. Chem. B* **2004**, *108*, 6603.
[96] N. Juranić, V. A. Likić, F. G. Prendergast, S. Macura, *J. Am. Chem. Soc.* **1996**, *118*, 7859.
[97] K. Krynicki, C. D. Green, D. W. Sawyer, *Faraday Discuss. Chem. Soc.* **1978**, *66*, 199.
[98] A. Giovannitti, C. B. Nielsen, J. Rivnay, M. Kirkus, D. J. Harkin, A. J. White, H. Sirringhaus, G. G. Malliaras, I. McCulloch, *Adv. Funct. Mater.* **2016**, *26*, 514.
[99] M. Bonomi, G. Bussi, C. Camilloni, G. A. Tribello, P. Banáš, A. Barducci, M. Bernetti, P. G. Bolhuis, S. Bottaro, D. Branduardi, R. Capelli, P. Carloni, M. Ceriotti, A. Cesari, H. Chen, W. Chen, F. Colizzi, S. De, M. De La Pierre, D. Donadio, V. Drobot, B. Ensing, A. L. Ferguson, M. Filizola, J. S. Fraser, H. Fu, P. Gasparotto, F. Luigi Gervasio, F. Giberti, et al., *Nat. Methods* **2019**, *16*, 670.
[100] G. A. Tribello, M. Bonomi, D. Branduardi, C. Camilloni, G. Bussi, *Comput. Phys. Commun.* **2014**, *185*, 604.
[101] M. Bonomi, D. Branduardi, G. Bussi, C. Camilloni, D. Provasi, P. Raiteri, D. Donadio, F. Marinelli, F. Pietrucci, R. A. Broglia, M. Parrinelloa, *Comput. Phys. Commun.* **2009**, *180*, 1961.
[102] Y. Osada, J. Ping Gong, Y. Tanaka, *J. Macromol. Sci., Part C: Polym. Rev.* **2004**, *44*, 87.
[103] P. Arosio, A. Famulari, M. Catellani, S. Luzzati, L. Torsi, S. V. Meille, *Macromolecules* **2007**, *40*, 3.
[104] P. Arosio, M. Moreno, A. Famulari, G. Raos, M. Catellani, S. V. Meille, *Chem. Mater.* **2009**, *21*, 78.
[105] N. Kayunkid, S. Uttiya, M. Brinkmann, *Macromolecules* **2010**, *43*, 4961.
[106] O. Alexiadis, V. G. Mavrantzas, *Macromolecules* **2013**, *46*, 2450.
[107] S. Hugger, R. Thomann, T. Heinzel, T. Thurn-Albrecht, *Colloid Polym. Sci.* **2004**, *282*, 932.
[108] M. Brinkmann, J.-C. Wittmann, *Adv. Mater.* **2006**, *18*, 860.
[109] Z. Wu, A. Petzold, T. Henze, T. Thurn-Albrecht, R. H. Lohwasser, M. Sommer, M. Thelakkat, *Macromolecules* **2010**, *43*, 4646.
[110] S. Himmelberger, A. Salleo, *MRS Commun.* **2015**, *5*, 383.
[111] M. Moser, T. C. Hidalgo, J. Surgailis, J. Gladisch, S. Ghosh, R. Sheelamanthula, Q. Thiburce, A. Giovannitti, A. Salleo, N. Gasparini, A. Wadsworth, I. Zozoulenko, M. Berggren, E. Stavrinidou, S. Inal, I. McCulloch, *Adv. Mater.* **2020**, *32*, 2002748.
[112] R. K. Hallani, B. D. Paulsen, A. J. Petty, R. Sheelamanthula, M. Moser, K. J. Thorley, W. Sohn, R. B. Rashid, A. Savva, S. Moro, J. P. Parker, O. Drury, M. Alsufyani, M. Neophytou, J. Kosco, S. Inal, G. Costantini, J. Rivnay, I. McCulloch, *J. Am. Chem. Soc.* **2021**, *143*, 11007.
[113] A. A. Szumska, I. P. Maria, L. Q. Flagg, A. Savva, J. Surgailis, B. D. Paulsen, D. Moia, X. Chen, S. Griggs, J. T. Mefford, R. B. Rashid, A. Marks, S. Inal, D. S. Ginger, A. Giovannitti, J. Nelson, *J. Am. Chem. Soc.* **2021**, *143*, 14795.
[114] I. P. Maria, B. D. Paulsen, A. Savva, D. Ohayon, R. Wu, R. Hallani, A. Basu, W. Du, T. D. Anthopoulos, S. Inal, J. Rivnay, I. McCulloch, A. Giovannitti, *Adv. Funct. Mater.* **2021**, *31*, 2008718.